Size-induced moment formation on isolated Fe atoms embedded in a nanocrystalline Ta matrix: Experiment and theory

S. K. Mohanta, S. N. Mishra,* Subhrangsu Sarkar, and Pushan Ayyub
Tata Institute of Fundamental Research (TIFR), Homi Bhabha Road, Mumbai-400005, India
(Received 1 May 2014; revised manuscript received 2 June 2014; published 16 June 2014)

Employing the time differential perturbed angular distribution (TDPAD) technique, we have measured the local susceptibility (χ_{loc}) of isolated Fe probe atoms implanted in nanocrystalline α-Ta as well as β-Ta host matrices. While Fe dopants in bulk Ta and β-Ta exhibit no magnetic response, the temperature dependence of χ_{loc} in nanocrystalline α-Ta reveals the emergence of a local magnetic moment on Fe below a critical size of $\approx$8 nm. Using *ab initio* electronic structure calculations, we show that the moment formation in nanocrystalline α-Ta occurs due to Stoner enhancement arising from an unusual size-dependent lattice expansion that results in a shift in the Fermi level.

DOI: 10.1103/PhysRevB.89.224410 PACS number(s): 75.20.Hr, 76.80.+y, 71.15.Mb, 75.75.−c

I. INTRODUCTION

The plethora of proven and potential applications of nanocrystalline materials makes it imperative to achieve a sound conceptual understanding of the size dependence of a variety of physicochemical properties. While the influences of quantum size effects [1,2] and surface effects on various physical properties of nanoparticles are relatively well understood, the often crucial effect of size-dependent changes in the lattice symmetry and lattice parameters [3] have not been investigated in detail. Size-dependent structural modifications have been known to play a key role, for example, in controlling the ferroelectric properties of perovskite materials [4]. Though the magnetic properties of nanoparticles have been studied in detail [5], finite size effects in the formation and stability of local magnetic moments, especially for isolated impurities, have received very little attention. Interestingly, the formation of local moments on isolated dopant atoms in a *nanocrystalline* host lattice have recently been found to show a marked size dependence that appears to be governed principally by structural modifications of the above type [6].

Over the past decades, extensive studies have been carried out on the magnetic behavior of many $3d$, $4d$, and $4f$ impurities in several bulk metallic hosts [7–11]. In comparison, much less is known about the nature of moment formation on single impurity atoms in naonostructured metallic hosts. Some of the basic issues that need to be addressed in this context are: (i) Does the finite size of the host matrix *in general* affect single impurity local magnetism, particularly when the same dopant is nonmagnetic in the same host matrix in the bulk? (ii) What is the underlying mechanism of moment formation (in the cases where it does occur)? (iii) And will such a moment be stable against spin fluctuations? The formation of a localized magnetic moment for an impurity embedded in a metallic host is governed by the condition $IN_l(E_F) \geqslant 1$, where I is the Stoner exchange parameter and $N_l(E_F)$ is the impurity paramagnetic local density of states at the Fermi energy E_F [12]. The stability of the moment depends on the spin fluctuations arising from Kondo interaction between the impurity-d (or f) electrons and the conduction band electrons of the host.

Nuclear techniques such as γ-ray time differential perturbed angular distribution (TDPAD) in conjunction with ion implantation have proved useful in the study of quasi-isolated impurity magnetism in a variety of hosts including, lately, nanocrystalline solids [6,13]. Finite size effects on local magnetism and Kondo interaction of isolated Fe dopants has been studied in nanocrystalline Cu, Ag, and Nb hosts [6,13]. The results revealed a strong influence of the particle size on the local magnetism of the Fe dopant, especially on the Kondo temperature. More interestingly, an investigation of Fe-implanted nanocrystalline Nb showed the emergence of a local moment below a critical size of 11 nm [6]. In spite of a few such recent developments, the amount of data available is not sufficient to settle basic questions on the precise role of lattice size on the magnetism of a dopant atom. It is therefore important to carry out studies of $3d$ magnetic atoms dispersed in other nanocrystalline hosts. The electronic and crystal structure (body centered cubic, bcc) of elemental α-Ta are similar to those of Nb. The metastable β-Ta phase with a body centered tetragonal (bct) structure can be stabilized when prepared in the form of thin films [14]. It is also known that Fe impurities in bulk Ta host are nonmagnetic [9]. Thus, a dilute dispersion of Fe atoms in nanocrystalline Ta hosts is a system well suited to the investigation of the possible formation of size-dependent local moments.

In this paper we report the magnetic behavior of isolated dilute Fe dopants in nanocrystalline α and β phases of Ta, as revealed by measurements of the local susceptibility using the TDPAD method. While Fe atoms in bulk and β-Ta show clearly nonmagnetic behavior, we observe a Curie-Weiss type local susceptibility for Fe in nanocrystalline α-Ta thin films with a mean grain size $\leqslant$8 nm, reflecting local moment formation on Fe. The observation of local moments below a critical size is independently supported by *ab initio* electronic structure calculations which indicate a Stoner enhancement arising from a size-dependent tuning of the Fermi level, leading to moment formation at and below $\approx$8 nm.

II. EXPERIMENTAL DETAILS

Nanocrystalline Ta thin films ($\approx$1 μm thick) were deposited on 250 μm thick Si (111) substrates by rf (for α-Ta) and dc (for β-Ta) magnetron sputtering from a 99.99% pure Ta target in an

*mishra@tifr.res.in

 ©2014 American Physical Society

argon atmosphere. In this process, the mean particle sizes can be varied by controlling the sputtering gas pressure, applied power, and substrate temperature [15]. The α-Ta films were deposited at an applied rf power of 100 W with a fixed target-to-substrate distance of 50 mm. The mean particle size was varied by changing the deposition pressure (5–100 mtorr) and the substrate temperature (25–600 °C). dc magnetron sputtering at room temperature with a high deposition current (250 mA) and low Ar pressure (5 mtorr) was used to deposit β-Ta thin films. Within the parameter space explored, it was not possible to vary the mean size of the β-Ta films to any large degree. The mean particle size of the samples was obtained in terms of the coherently diffracting domain size (d_{XRD}) from x-ray diffraction (XRD) line broadening of the [110] reflection, after subtracting the instrumental broadening and strain broadening using the Scherrer formula [16].

TDPAD experiments were carried out at the Pelletron Accelerator Facility at TIFR. The magnetic response of Fe atoms in the host of interest was studied via hyperfine interaction of the 10^+ isomeric state of the ^{54}Fe nucleus ($T_{1/2} = 360$ ns, $g_N = 0.728$) [17] produced by the reaction $^{45}\mathrm{Sc}(^{12}\mathrm{C},p2n)^{54}\mathrm{Fe}$. The recoiling ^{54}Fe nuclei were implanted deep ($\approx$1 μm) inside the host matrix at concentrations well below 1 ppm [6]. Measurements were performed within a time window of 10 ns to 1 μs immediately after implantation. These experimental conditions ensure negligible impurity-impurity interaction and the results reflect the magnetic response of a truly isolated impurity. Observations were made in the temperature range of 15–300 K and in an applied magnetic field of 2 T and the data were collected using high purity Ge γ-ray detectors placed at $\pm45^\circ$ and $\pm135^\circ$ with respect to the beam direction. The energy gated time spectra of the γ rays decaying from the isomeric state were used to construct the spin rotation spectra $R(t)$ defined as [6]

$$R(t) = \frac{N(+\theta,t) - N(-\theta,t)}{N(+\theta,t) + N(-\theta,t)}.$$

Here $N(\theta,t)$ is the background corrected and normalized count rate for the detector placed at an angle θ. The spectra obtained for the detector pairs at $\pm135^\circ$ and $\mp45^\circ$ were summed and fitted to the function

$$R(t) = (-3/4)A_{22}e^{-t/\tau_N}\sin(2\omega_L t - \phi)f(\omega\tau_r)$$

to extract the Larmor precession frequency ω_L and nuclear relaxation time τ_N. Here A_{22} is the anisotropy of the angular distribution pattern and ϕ is the phase factor arising from a finite bending of the incoming beam in the applied field. The factor $f(\omega\tau_r) = \exp(-\omega^2\tau_r^2/2)$ accounts for attenuation of $R(t)$ due to finite time resolution of the detectors. Using the relation $\omega_L = (g_N\mu_N B_{\mathrm{eff}}/\hbar)$, one can estimate the effective magnetic field $B_{\mathrm{eff}} = B_{\mathrm{ext}} + B_{\mathrm{hf}}$ and hence the hyperfine field B_{hf} at the probe nuclear site. For paramagnetic systems, B_{hf} is proportional to the external field, while the ratio $\beta = B_{\mathrm{eff}}/B_{\mathrm{ext}}$ gives a measure of the local susceptibility $\chi_{\mathrm{loc}}(\equiv \beta - 1)$ of the probe. Further details about the TDPAD experiments can be found elsewhere [18,19].

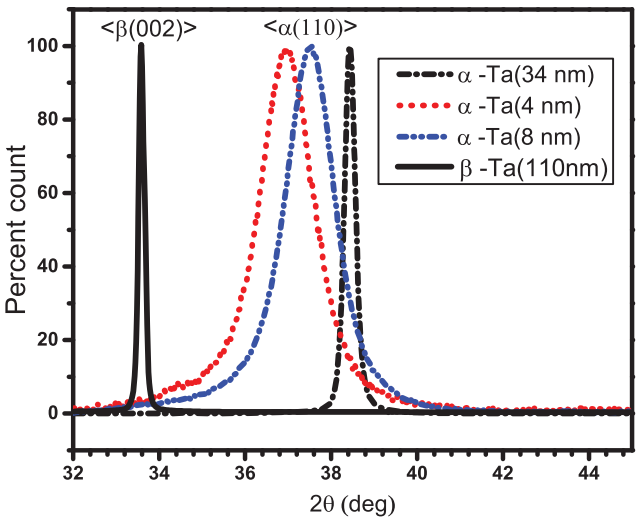

FIG. 1. (Color online) X-ray diffraction patterns of three α-Ta films and one β-Ta film. The Scherrer size (coherently diffracting domain size, d_{XRD}) corresponding to each sample is indicated.

III. RESULTS AND DISCUSSION

Figure 1 shows the XRD patterns of three α-Ta samples with $4 \leqslant d_{\mathrm{XRD}} \leqslant 34$ nm and one β-Ta sample with $d_{\mathrm{XRD}} \approx 110$ nm, which were subsequently used for TDPAD measurements. The diffraction line in the 2θ range 36°–40° was identified to be the [110] reflection of α-Ta (bcc, space group 221), while the sharp line near $2\theta \approx 33.75^\circ$ corresponds to the [002] reflection of β-Ta (bct, space group 113). The tetragonal lattice parameters of the bct phase (β-Ta) were found to be $a = 10.194$ Å and $c = 5.131$ Å, in good agreement with earlier results [14]. In the case of α-Ta, it is clear from Fig. 1 that with a reduction in the particle size, the (110) diffraction line shifts consistently to lower 2θ values, indicating a size-induced expansion of the unit cell. The lattice constant of this phase increases from 3.301 Å in bulk Ta to 3.495 Å in nano-Ta with $d_{\mathrm{XRD}} = 4$ nm.

The microstructure of the α-Ta samples was also examined using field emission electron microscopy (FESEM). Typical electron micrographs for the three samples are displayed in Fig. 2. Note that the microstructure reveals the aggregate particle size, which is usually larger than the crystallographic domain size given by d_{XRD}.

Figure 3 shows the typical spin rotation spectra $R(t)$ and their Fourier transforms for ^{54}Fe in bulk and nanocrystalline Ta hosts. The spectra exhibit well defined oscillations with high anisotropy, suggesting that the implanted Fe atoms came to rest at regular, probably substitutional lattice sites. The spectra recorded for the nanocrystalline α-Ta samples could be fitted with a single Larmor frequency ω_L, which indicates that most of the Fe atoms were located at regular lattice sites within the nanoparticles. We point out that the depth profile of the implanted Fe ions obtained from the Monte Carlo simulation package SRIM [20] was found to be $\approx$0.8 μm, with a distribution width of 0.2 μm due to straggling. This suggests that most of the ^{54}Fe atoms stop inside the nanocrystalline Ta films. Figure 4 shows the local susceptibility of Fe, $\chi_{\mathrm{loc}}(T)$, in bulk and nano-Ta. The local susceptibility data observed for bulk Ta and the nanocrystalline sample with

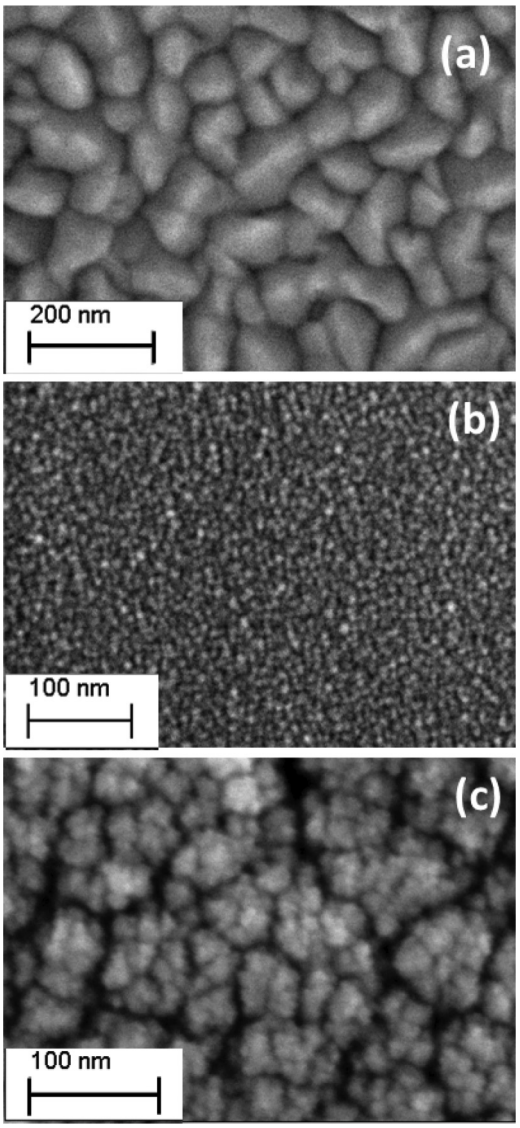

FIG. 2. Field emission scanning electron micrographs of three α-Ta films corresponding to the Scherrer sizes: (a) 34 nm, (b) 8 nm, and (c) 4 nm.

particle size = 34 nm reflect nonmagnetic behavior of Fe with $\beta(T) \sim 1$. However, on further reducing the particle size, the local susceptibility showed significant deviation from the nonmagnetic behavior with $\beta(T) < 1$. Furthermore, for the smaller nanoparticles ($\leqslant$8 nm), $\beta(T)$ showed a strong temperature dependence. This clearly indicates the presence of a local magnetic moment on the Fe atoms in nanocrystalline Ta with $d_{\mathrm{XRD}} \leqslant 8$ nm. The spin rotation spectrum recorded for the β-Ta film showed a nonmagnetic response with $\beta(T) = 1$. Importantly, this indicates that the magnetic response observed in the smaller-sized α-Ta samples cannot be due to the presence of small amounts of β-Ta impurity that might have remained undetected by XRD.

The $\chi_{\mathrm{loc}}(T)$ data for Fe in the α-Ta nanoparticles could be fitted to the Curie-Weiss law: $\chi_{\mathrm{loc}}(T) = C/(T + T_K)$, where the Curie constant $C = g\mu_B(S+1)B(0)/3k_B$ provides a measure of the Fe magnetic moment $\mu_{\mathrm{Fe}} = gS$. Here T_K is the Kondo temperature, $B(0)$ is the magnetic hyperfine field at

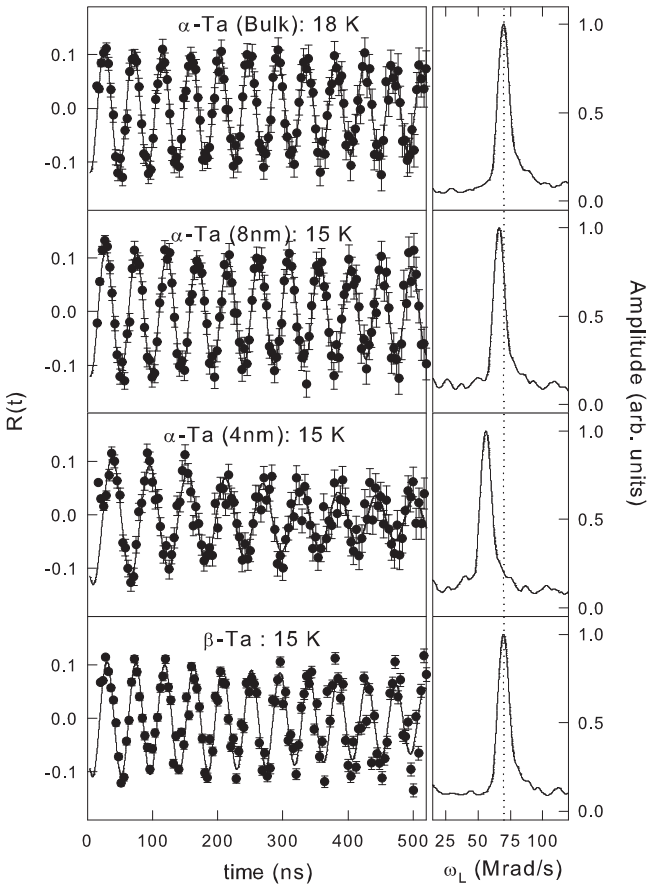

FIG. 3. Spin rotation spectra $R(t)$ recorded at 15 K (left panel) and their Fourier transforms (right panel) for ^{54}Fe in nanocrystalline Ta with varying particle size d_{XRD}. The bottom panel corresponds to Fe in β-Ta.

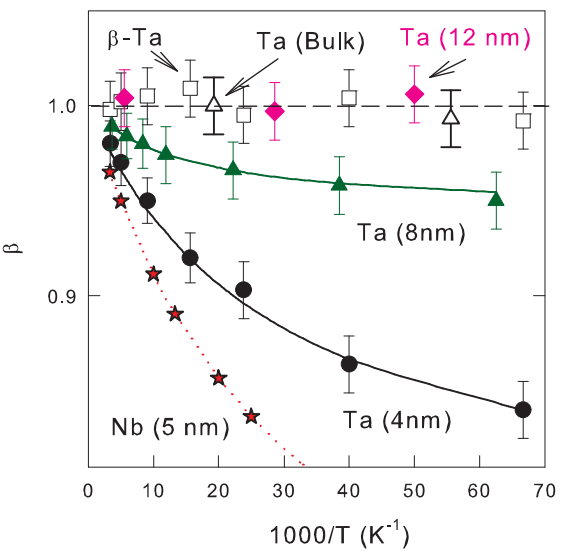

FIG. 4. (Color online) Temperature dependence of the local susceptibility $\beta(T)$ of ^{54}Fe in bulk and nanocrystalline Ta. Data for Fe in 5 nm nano-Nb (stars) taken from Ref. [9] are shown for comparison. The solid and dotted lines represent a fit to Curie-Weiss law discussed in the text.

TABLE I. Curie constant C, Kondo temperature T_K, and magnetic moment $\mu_{\rm Fe}^{\rm expt}$ of Fe in nanocrystalline Ta obtained from TDPAD. The Fe moments ($\mu_{\rm Fe}^{\rm calc}$) and hyperfine fields ($B_{\rm hf}^{\rm calc}$) are obtained from *ab initio* calculations (see text). $m1$, $m2$, and $m3$ are the induced moments on the host Ta atoms in the three nearest neighbor shells of the Fe probe atom.

Host	C (K)	T_K (K)	$\mu_{\rm Fe}^{\rm expt}$ (μ_B)	$\mu_{\rm Fe}^{\rm calc}$ (μ_B)	$B_{\rm hf}^{\rm calc}$ (kG)	$m1$ (μ_B)	$m2$ (μ_B)	$m3$ (μ_B)
Bulk Ta	0	–	0					
34 nm α-Ta	0	–	0					
12 nm α-Ta	0	–	0					
8 nm α-Ta	−3.2(7)	89(20)	0.6(2)	0.76	−56	0.02	−0.03	−0.003
4 nm α-Ta	−8.0(4)	35(10)	1.7(2)	1.83	−97	0.06	−0.05	−0.007
110 nm β-Ta	0	–	0		0			

$T = 0$, and S is the effective spin on Fe. The derived values of C and T_K are summarized in Table I. It is interesting to note that a reduction in the size causes an increase in C and decrease in T_K. The magnetic moments $\mu_{\rm Fe}$ of Fe in nanosized α-Ta were estimated (see Table I) using the values of $B(0)$ obtained from *ab initio* calculations, discussed below. Our data clearly indicate that the local moment that appears on the Fe atoms in nano-Ta at and below 8 nm progressively increases with a reduction in the particle size, while the Kondo temperature T_K decreases, reflecting suppression of the spin fluctuation rate.

Information regarding the spin fluctuation of Fe-3d moment in the Ta nanoparticles can be obtained from nuclear spin relaxation time τ_N extracted from the damping of the spin rotation spectra [6]. For an isolated magnetic impurity embedded in a metallic host, the observed damping is related to the spin fluctuation rate τ_J^{-1} via the Abragam-Pound relation [21] $\tau_J^{-1} = 2(g_N\mu_N/\hbar)^2 B(0)^2 (S+1) S^{-1} \tau_N$, whose temperature dependence follows the Korringa relation $\tau_J^{-1} = 4\pi\hbar^{-1}(J_{\rm ex}\rho)^2 k_B T$ [22]. Here $J_{\rm ex}$ is the exchange interaction between the magnetic moment of the impurity atom and ρ is the density of states at the Fermi energy E_F. The temperature dependence of the observed nuclear relaxation times (τ_N) for ^{54}Fe in bulk and nanocrystalline Ta samples are displayed in Fig. 5. From the $R(t)$ spectra shown in Fig. 3, we notice that the nuclear spin relaxation times for bulk and larger Ta nanoparticles (34 nm) are quite long ($\tau_N \geqslant 3600$ ns). In contrast, the spectra recorded for the smaller nanoparticles, especially for the 4 nm sample, show strong damping with τ_N becoming smaller at lower temperatures. While $\tau_N(T)$ for the bulk and larger sized (34 nm) nanoparticles remain temperature independent, the damping observed for small particle sizes ($\leqslant$8 nm) linearly increases with decreasing temperature reflecting Korringa type behavior: $\tau_N \propto \tau_J^{-1} \propto T$. We note that the observed damping parameter could have a contribution from the static broadening of ω_L due to the nonidentical local environment of the probe atoms. However, considering the Curie-Weiss type local susceptibility and the Korringa-like temperature dependence of τ_N, it is reasonable to assume that dominant contribution to the relaxation of the spin rotation comes from dynamic fluctuation of the Fe moment. From the relation [22] $T_K = T_F e^{-1/(J_{\rm ex}\rho)}$ and using the value for $(J_{\rm ex}\rho)$ obtained from the slope of the $\tau_N(T)$ data, we estimate the Kondo temperatures as $T_K = 30$ and 81 K for the 4 and 8 nm samples, respectively, which are close to the values extracted from the $\chi_{\rm loc}(T)$ data (Table I). The above analysis, though based on the Kondo model valid for nondegenerate d impurities, reproduces the observed values of T_K reasonably well. This indicates that corrections due to on-site Coulomb correlation, applicable for degenerate Fe-d states, may not be significant enough in these systems to influence the main conclusions of our study.

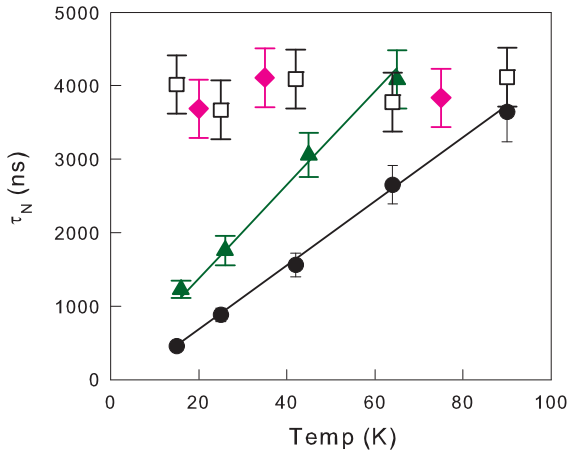

FIG. 5. (Color online) Temperature dependence of the nuclear spin relaxation time τ_N of ^{54}Fe in nanocrystalline Ta samples. The solid line correspond to a linear fit reflecting Korringa behavior. Symbols have the same significance as in Fig. 4.

To complement and understand the experimental results, we have performed *ab initio* electron structure calculations within the framework of density functional theory (DFT) [23–25], using the all electron full-potential augmented plane wave + local orbital (APW + lo) technique [25–27] as implemented in the WIEN2k package [28]. The calculations were carried out using a 54-atom supercell (53 Ta + 1 Fe) constructed with 27 units ($3 \times 3 \times 3$) of bcc Ta with the experimentally observed lattice constants for the nanoparticles. In the APW + lo method, the wave functions are expanded in spherical harmonics inside nonoverlapping atomic spheres of radius $R_{\rm MT}$, and in plane waves in the remaining space of the unit cell (the interstitial region). The muffin-tin radii for Fe and Ta were chosen as $R_{\rm MT} = 2.3$ and 2.5 a.u., respectively. The maximum angular momentum for the expansion of the wave function in spherical harmonics inside the atomic spheres was taken to be $\ell_{\rm max} = 10$. The plane wave expansion in the interstitial region was made up to a cut-off wave vector set to

be $K_{max} = 7.5/R_{MT}^{min} = 3.26$ a.u.$^{-1}$. The charge density was Fourier expanded up to $G_{max} = 16\sqrt{Ry}$. For the sampling of the Brillouin zone, a k mesh of size $10 \times 10 \times 10$ was used. As exchange-correlation functional, the Perdew-Burke-Ernzerhof [29] generalized gradient approximation (GGA) was used and calculations were performed with and without spin polarization, the latter corresponding to the nonmagnetic situation. In each of the cases studied, full lattice relaxation was allowed to minimize the force below 0.1 Ry/Å and self-consistency was obtained with the energy and charge convergence criterion set to 0.1 mRy and 0.0001, respectively.

Figure 6 displays the local density of states (LDOS) for the Fe impurity obtained from unpolarized and spin polarized calculations. We first discuss the results from the nonmagnetic calculations and examine the Stoner condition for moment formation. Taking the Stoner exchange parameter $I = 0.9$ eV for Fe [12], we find that a local moment can exist only when $N_{Fe}(E_F) \geqslant 1.1$ states/eV atom. The LDOS results (Fig. 6) show that the occupied $3d$-t_{2g} states of Fe in the bulk Ta host, strongly overlapping with the Ta-4d band, are piled up near -1.5 eV, while the empty d-e_g states are pushed above E_F. As a result, the DOS for Fe at the Fermi energy turns out to be rather small, $N_{Fe}(E_F) \approx 0.9$ states/eV atom. In the case of nano-Ta, the Fe LDOS does not show appreciable change down to 34 nm (see Fig. 6). Since $N_{Fe}(E_F)$ is less than the Stoner limit, the Fe atoms are expected to be nonmagnetic in nano-Ta down to $\approx$10 nm, in agreement with our experimental results. With a further reduction in size, the Fermi level shifts to lower energies, resulting in a shift of the Fe $3d$-t_{2g} band towards E_F together with a decrease of its bandwidth (Fig. 6). Note that for the 8 nm case, the LDOS shows a weak resonance (virtual bound state) at E_F, whose spectral weight increases with decreasing size. Consequently, $N_{Fe}(E_F)$ increases to values larger than the Stoner limit: $N_{Fe}(E_F) = 2.2$ and 1.4 states/eV atom for particle size of 4 and 8 nm, respectively. These calculations, shown in Fig. 6, clearly indicate that local moment formation is favored for Fe in nanoparticles of cubic Ta with size $\leqslant$8 nm, corroborating our TDPAD observations.

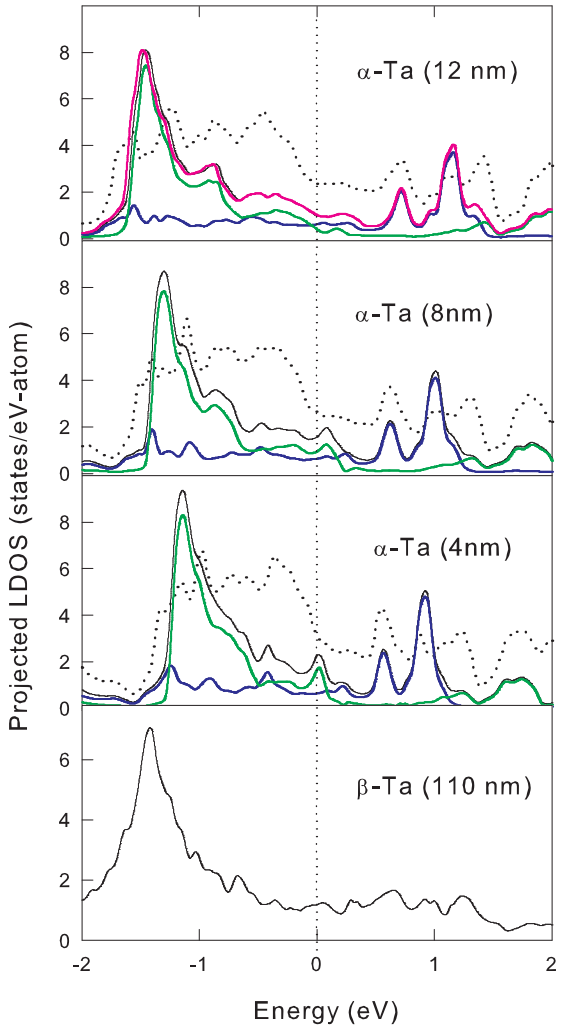

FIG. 6. (Color online) Projected nonmagnetic density of states (DOS) for Fe impurity in bulk and nano-Ta hosts. Colored lines represent: black = Fe-d, green = t_{2g}, blue = e_g, and dotted black = Ta-d (×5). The pink line in the topmost panel corresponds to Fe in bulk Ta and the red line in the lowest panel represents Fe-d DOS in β-Ta. Vertical dotted line shows the position of the Fermi energy E_F.

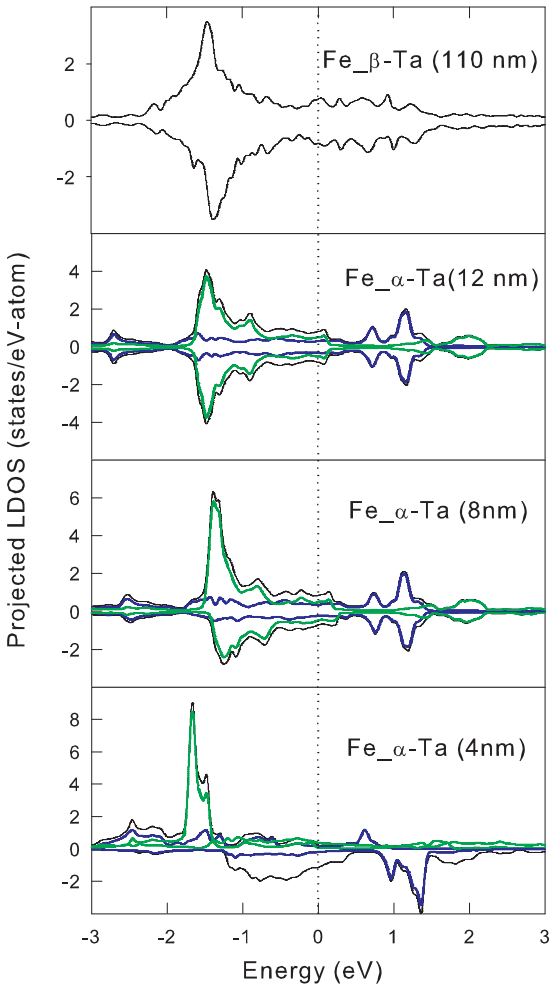

FIG. 7. (Color online) Spin resolved d-projected density of states for Fe impurity in bulk and nano-Ta hosts. Color lines represent: black = Fe-d, green = t_{2g}, and blue = e_g. Vertical dotted line at zero energy shows the position of the Fermi energy.

The onset of a local moment for Fe in nano-Ta ($\leqslant$8 nm) is more clearly visible in the spin polarized LDOS of Fe (shown in Fig. 7), which begins to exhibit an exchange splitting that increases with decreasing size. The magnitude of the Fe moment, shown in Table I, increases from 0.76 μ_B at 8 nm to 1.83 μ_B at 4 nm, closely agreeing with the values of $\mu_{\rm Fe}$ estimated from the local susceptibility data. This also lends strong support to our earlier assertion that the Fe atoms occupy substitutional sites in the Ta hosts. We have also calculated the magnetic hyperfine field $B_{\rm hf}$ of Fe (Table I), which appears with the onset of local moment and expectedly increases with decreasing size. Thus, our *ab initio* calculations reveal a strong influence of the Ta lattice size on the magnetism of Fe, exhibiting a crossover from nonmagnetic to local moment behavior below a critical size of $\approx$8 nm. Similar calculations performed for Fe in β-Ta (see top panel in Fig. 7) show no spin splitting for Fe-d, corroborating the nonmagnetic behavior reflected by our experimental results. This is consistent with the expected behavior, considering that the near neighbor distances in β-Ta are much smaller than in α-Ta, which would lead to much stronger d-d hybridization and hence higher spin fluctuation leading to the observed absence of magnetic response.

In order to test the validity of our simple model, we carried out calculations within the GGA + U formalism for the 4 nm nano Ta sample. These took account of the on-site Coulomb correlation with self-interaction correction (SIC) and spin-orbit interaction [30,31]. We assume the Coulomb correlation U for Fe to be in the range 2–3 eV and the exchange energy $J = 0.9$ eV [32,33]. We find that, within the atomic sphere of the Fe impurity, the calculated value of the orbital moment is negligible ($\approx$0.04 μ_B), while the spin moment is almost the same ($\approx$1.68 μ_B) as obtained from pure GGA. We therefore conclude that the effect of on-site Coulomb interaction is unimportant for the system considered here.

Figure 8 displays the size-dependent evolution of the Fe magnetic moment ($\mu_{\rm Fe}$) in the nano-Ta host, together with the experimentally measured Curie constant and the calculated $N(E_F)$. The crossover from nonmagnetic to local moment behavior of the Fe probe atom below a critical size of $\approx$8 nm is clearly brought about by the size-dependent narrowing of the Fe-d band coupled with a shift of the Fermi level that results in a large increase in $N(E_F)$, thereby satisfying the Stoner criterion. It is instructive to compare the magnetic response

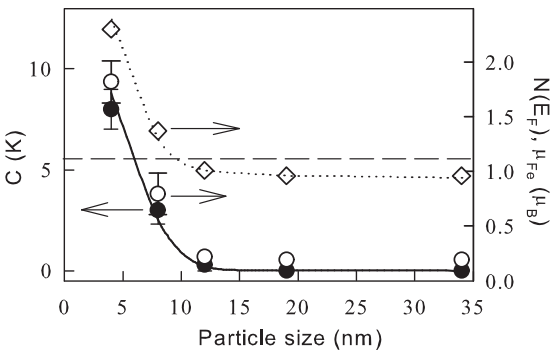

FIG. 8. Dependence of the Curie constant (•), Fe moment (○), and $N(E_F)$ (◇) with a particle size of nano-Ta samples. Lines are visual guides.

of Fe in nanocrystalline Ta with that in nanocrystalline Nb [6], a closely related system. Though the behavior of Fe in nano-Ta and nano-Nb are qualitatively similar, there are subtle and interesting differences. For instance, as shown in Fig. 4, the local susceptibility of Fe in nano-Ta is significantly lower than that in nano-Nb with comparable crystallite size, indicating a smaller local moment in the former. This is also corroborated by our calculations. A similar trend is seen for the Kondo temperatures listed in Table I. These observations are in accordance with the fact that hybridization of Fe-d in Ta is higher than that in Nb. Second, the critical size for local moment formation in nano-Ta ($\approx$8 nm) is slightly lower than that in nano-Nb ($\approx$12 nm). This can be traced to the hybridization of Fe-3d with Ta-5d states being much larger than that with Nb-4d states. Hence, it requires a larger lattice expansion (smaller particle size) for the Fe moment to appear.

Next we examine the effect of lattice size on the spin fluctuation of the Fe moments and argue that the host spin polarization has a strong influence on the Kondo temperature T_K. According to the Kondo model [22], the local moment of the impurity atom produces a negative spin polarization of the host conduction electrons, resulting in an effective loss (screening) of the moment below T_K. Alternately, the antiferromagnetic exchange interaction between the local moment and the conduction electrons causes the local moment to fluctuate and the time averaged moment appears to diminish below T_K, whose value depends on the interaction strength $J\rho \approx |V_{kd}|^2\rho/\epsilon_d$. Here V_{kd} is the hybridization strength, ϵ_d is the position of the Fe-3d resonance relative to E_F, and ρ is the host DOS at E_F. A rough estimation, using the formalism given in Refs. [33,34] yields $|V_{kd}| \approx 0.52$ eV for Fe in 4 nm nano-Ta, in accordance with the width of the Fe-d band in Fig. 6. For larger Ta particles, V_{kd} is expected to be even higher because of smaller interatomic distance. Assuming ϵ_d to be $\approx$0.6 eV (centroid of the Fe-3d band) and taking ρ to be the same as that of bulk Ta, the exchange interaction $J\rho$ comes out as ≈ -0.40. This implies that Fe atoms in nano-Ta hosts should be nonmagnetic with a high $T_K \geqslant 5 \times 10^3$ K, which contradicts our observation of a large $\mu_{\rm Fe}$ and low T_K in 4 nm Ta nanoparticles.

How do we understand the reduction of Kondo temperature in spite of a large hybridization strength? We believe that a positive spin polarization of the host conduction band electrons gives rise to a ferromagnetic exchange interaction between Fe-3d host conduction electrons and effectively lowers the Kondo temperature. Information regarding host spin polarization produced by Fe in nano-Ta can be obtained by examining the induced moments at the host-Ta atoms surrounding the Fe impurity. Referring to the results obtained from our *ab initio* calculations (see Table I), we note that the Fe impurity moment induces a small but positive polarization, indicating ferromagnetic d-d interaction between Fe and host conduction electrons. The host atoms further away from the impurity show negative spin polarization. The magnitude of the ferromagnetic spin polarization increases with decreasing particle size. These calculations qualitatively support our proposition that a positive host spin polarization can effectively diminish the Kondo coupling $J\rho$ and thus suppress spin fluctuations resulting in a lower T_K, as also observed in several other dilute systems [6,10,11,13,35].

In summary, we have studied the local magnetism of isolated Fe probe atoms in nanocrystalline Ta hosts. Measurements of the local susceptibility and 3*d* spin relaxation rates, combined with *ab initio* electronic structure calculations, show a strong influence of lattice size on the Fe magnetism. We have shown that a size-induced lattice expansion in nano-Ta shifts the Fermi level and causes large enhancements in the local density of states, allowing the formation of local moments on Fe atoms below a critical size of 8 nm. The relatively low value of the Kondo temperature observed for Fe in nano-Ta possibly arises from a ferromagnetic spin polarization of the host conduction band electrons. These results should prove to be important for an improved understanding of the magnetic behavior of isolated impurities in metallic hosts at reduced dimensions.

[1] W. P. Halperin, Rev. Mod. Phys. **58**, 533 (1986).
[2] A. D. Yoffe, Adv. Phys. **50**, 1 (2001).
[3] P. Ayyub, V. R. Palkar, S. Chattopadhyay, and M. S. Multani, Phys. Rev. B **51**, 6135 (1995).
[4] S. Chattopadhyay, P. Ayyub, V. R. Palkar, and M. S. Multani, Phys. Rev. B **52**, 13177 (1995).
[5] R. H. Kodama, J. Magn. Magn. Mater. **200**, 359 (1999).
[6] S. N. Mishra, S. K. Mohanta, S. M. Davane, N. Kulkarni, and P. Ayyub, Phys. Rev. Lett. **105**, 147203 (2010).
[7] K. H. Fisher, in *Numerical Data and Functional Relationships in Science and Technology*, edited by K. H. Hellweg and J. L. Oslen, Landolt-Bornstein, New Series Group III, Vol. 15 (Springer, Berlin, 1982), p. 289.
[8] A. C. Hewson, *The Kondo Problem to Heavy Fermion* (Cambridge University Press, Cambridge, 1993).
[9] D. Riegel, L. Büermann, K. D. Gross, M. Luszik-Bhadra, and S. N. Mishra, Phys. Rev. Lett. **62**, 316 (1989).
[10] S. Khatua, S. N. Mishra, S. H. Devare, and H. G. Devare, Phys. Rev. Lett. **68**, 1038 (1992).
[11] A. A. Tulapurkar, S. N. Mishra, R. G. Pillay, H. G. Salunke, G. P. Das, and S. Cottenier, Phys. Rev. Lett. **85**, 1978 (2000).
[12] T. Beuerle, K. Hummler, C. Elsässer, and M. Fähnle, Phys. Rev. B **49**, 8802 (1994).
[13] S. N. Mishra, S. Bose, P. Vasa, and P. Ayyub, Phys. Rev. B **71**, 094429 (2005).
[14] M. H. Read and C. Altman, Appl. Phys. Lett. **7**, 51 (1965).
[15] R. Chandra, P. Taneja, J. John, P. Ayyub, G. K. Dey, and S. K. Kulshreshtha, Nanostruct. Mater. **11**, 1171 (1999).
[16] B. E. Warren, *X-ray Diffraction* (Addison-Wesley, Reading, MA, 1969), p. 251.
[17] N. J. Stone, Atomic Data Nuclear Data Tables **90**, 75 (2005).
[18] G. Schatz and A. Weidinger, *Nuclear Condensed Matter Physics* (Wiley, New York, 1996).
[19] H. E. Mahnke, Hyperfine Interact. **49**, 77 (1989).
[20] J. F. Ziegler, M. D. Ziegler, and J. P. Biersack, Nucl. Instrum. Methods B **268**, 1818 (2010), and references therein.
[21] A. Abragam and R. V. Pound, Phys. Rev. **92**, 943 (1953).
[22] J. Kondo, in *Solid State Physics*, edited by F. Seitz, D. TurTaull, and H. Ehrenreich (Academic, New York, 1969), Vol. 23, p. 184.
[23] P. Hohenberg and W. Kohn, Phys. Rev. **136**, B864 (1964).
[24] W. Kohn and L. J. Sham, Phys. Rev. **140**, A1133 (1965).
[25] S. Cottnier, *Density Functional Theory and the Family of (L)APW-methods: A Step-By-Step Introduction* (Instituut voor Kern-en Stralingsfysica, K. U. Leuven, Belgium, 2013).
[26] E. Sjöstedt, L. Nordström, and D. J. Singh, Solid State Commun. **114**, 15 (2000).
[27] G. K. H. Madsen, P. Blaha, K. Schwarz, E. Sjöstedt, and L. Nordström, Phys. Rev. B **64**, 195134 (2001).
[28] P. Blaha, K. Schwarz, G. K. H. Madsen, D. Kvasnicka, and J. Luitz, *WIEN2k: An Augmented Plane Wave + Local Orbitals Program for Calculating Crystal Properties* (Karlheinz Schwarz, Technische Universität, Wien, Austria, 2001).
[29] J. P. Perdew, K. Burke, and M. Ernzerhof, Phys. Rev. Lett. **77**, 3865 (1996).
[30] V. I. Anisimov, J. Zaanen, and O. K. Andersen, Phys. Rev. B **44**, 943 (1991); A. I. Liechtenstein, V. I. Anisimov, and J. Zaanen, *ibid.* **52**, R5467 (1995).
[31] V. I. Anisimov, I. V. Solovyev, M. A. Korotin, M. T. Czyzyk, and G. A. Sawatzky, Phys. Rev. B **48**, 16929 (1993).
[32] S. Chadov, J. Minar, M. I. Katsnelson, H. Ebert, D. Ködderitzsch, and A. I. Liechtenstein, Europhys. Lett. **82**, 37001 (2008).
[33] D. van der Marel and G. A. Sawatzky, Phys. Rev. B **37**, 10674 (1988).
[34] W. A. Harrison and G. K. Straub, Phys. Rev. B **36**, 2695 (1987), and references therein.
[35] S. K. Srivastava, S. N. Mishra, and G. P. Das, J. Phys.: Condens. Matter **18**, 9463 (2006).